

Constraining particle dark matter using local galaxy distribution

Shin'ichiro Ando^a and Koji Ishiwata^b

^aGRAPPA Institute, University of Amsterdam, 1098 XH Amsterdam, The Netherlands

^bInstitute for Theoretical Physics, Kanazawa University, Kanazawa 920-1192, Japan

E-mail: s.ando@uva.nl, ishiwata@hep.s.kanazawa-u.ac.jp

Abstract. It has been long discussed that cosmic rays may contain signals of dark matter. In the last couple of years an anomaly of cosmic-ray positrons has drawn a lot of attentions, and recently an excess in cosmic-ray anti-proton has been reported by AMS-02 collaboration. Both excesses may indicate towards decaying or annihilating dark matter with a mass of around 1–10 TeV. In this article we study the gamma rays from dark matter and constraints from cross correlations with distribution of galaxies, particularly in a local volume. We find that gamma rays due to inverse-Compton process have large intensity, and hence they give stringent constraints on dark matter scenarios in the TeV scale mass regime. Taking the recent developments in modeling astrophysical gamma-ray sources as well as comprehensive possibilities of the final state products of dark matter decay or annihilation into account, we show that the parameter regions of decaying dark matter that are suggested to explain the excesses are excluded. We also discuss the constrains on annihilating scenarios.

Contents

1	Introduction	1
2	Extragalactic gamma rays from dark matter	2
2.1	Scenarios of (decaying) dark matter	3
2.2	Gamma rays from dark matter	4
3	Extragalactic gamma-ray background from astrophysical sources	8
4	Cross correlation between the extragalactic gamma-ray background with galaxy catalogs	9
5	Results	10
5.1	Analysis including dark matter component alone	10
5.2	Analysis including astrophysical sources and dark matter component	14
6	Conclusions	17
A	Energy loss rate due to inverse-Compton scattering	20

1 Introduction

Discovery of the Higgs boson at the CERN Large Hadron Collider (LHC) has confirmed the standard model of particle physics [1, 2]. To be precise the standard model is an effective theory below TeV scale, meanwhile the validity of the standard model above TeV scale has not been unveiled. In cosmology, on the other hand, the observation of the cosmic microwave background (CMB) strongly supports the cold dark matter with a cosmological constant (Λ CDM model), which indicates that about 26% of the total energy density of the universe is occupied by non-baryonic cold dark matter [3–5]. As well-known, however, the standard model cannot explain the existence of dark matter. While its energy density is precisely determined by the analysis of the CMB, the other properties, such as the mass, lifetime, spin, quantum numbers, etc., are still unknown. Weakly interacting massive particles (WIMPs) are considered to be a good candidate for dark matter. The reason is that the WIMPs are produced in thermal plasma in the early universe, and then their relic abundance can naturally fit to the observed density of dark matter if the mass is around the weak scale. In fact, one of the goals of the LHC experiment has been the observation of dark matter. However, since no signal of dark matter has been reported at the LHC so far, it may indicate that the interaction of dark matter with ordinary particles is extremely weak (*e.g.*, axion, very light gravitino or axino), or simply its mass is larger than TeV.

The observation of cosmic rays has a potential for the search of such classes of dark matter. Even if its mass is much larger than the energy scale of collider experiments, dark matter may annihilate or decay to produce lots of high-energy cosmic rays. Even in a case that dark matter extremely weakly interacts with the standard model particles, cosmic rays can still be produced if dark matter has finite lifetime. Gravitino or axino in supersymmetric models are well-motivated examples. For gravitino, since its interaction with ordinary particles is suppressed by the Planck scale, gravitino can be enough long-lived to explain dark

matter even under R_p violation [6]. In annihilation or decay of dark matter, variety of the cascading decay products could be observed as anomalous fluxes among the astrophysical cosmic rays. In fact some anomalous cosmic rays have been reported. The latest observations are given by AMS-02. They have shown an excess in positron flux which has a peak around 300 GeV [7]. In addition, they have also reported an excess in anti-proton flux in the same energy range [8]. If dark matter is the origin of these anomalous cosmic rays, the observations indicate that the mass of dark matter is 1–10 TeV. On the other hand, however, it is not necessary to attribute the excesses to dark matter. There are claims that it is possible to account for the anomalous positrons by pulsars (see, *e.g.*, ref. [9] for recent work) or anti-protons by known-galactic sources [10, 11]. These claims, however, do not completely exclude the dark matter hypothesis for the anomalous cosmic rays.

In this article, we mainly investigate the dark matter scenarios which claim to explain the anomalous positron or anti-proton in light of cross correlation between gamma rays from dark matter and the observed galaxies. It was pointed out that the inverse-Compton (IC) process gives large amount of gamma rays in decaying [12] or annihilating [13] dark matter, and recently ref. [14] has updated the constraints on decaying dark matter by using the *spectral* data of 50-month extragalactic gamma-ray background (EGRB) by Fermi-LAT [15]. On the other hand, however, the IC process has not been taken into account in the previous studies using the *cross-correlation* of the gamma rays [16, 17]. We therefore include the IC gamma rays in the cross correlation analysis, which is shown to be essential for constraining decay lifetimes or annihilation cross sections for heavy mass dark matter particularly for leptonic channels. We also investigate more final states than in the previous works. Since the decay signal does not depend on the clustering of dark matter, robust constraints are obtained since gamma rays from dark matter can be computed with little uncertainties for each of decaying dark matter scenarios.¹ It will be shown that the decaying dark matter scenarios to explain the cosmic-ray positron or anti-proton excess are excluded. For the annihilating scenario, on the other hand, we will show that the constraints can be competitive with other probes such as dwarf spheroidal galaxies [19] by adopting reasonable parameters for abundance of dark matter halos and subhalos.

In this paper, we use the following cosmological parameters: Hubble constant $H_0 = 67.81 \text{ km s}^{-1} \text{ Mpc}^{-1}$ with $h = 0.6781$, density parameter of dark matter $\Omega_{\text{dm}} h^2 = 0.1186$ [5]. The critical density is obtained from Hubble parameter, $\rho_c = 1.054 \times 10^{-5} h^2 \text{ GeV cm}^{-3}$.

2 Extragalactic gamma rays from dark matter

In this section we explain how to compute the EGRB intensity from dark matter. There are three components to determine gamma rays from dark matter in a decaying or annihilating scenario. One is the intrinsic gamma-ray energy spectrum per decay or annihilation. The others are mass m_{dm} and lifetime τ_{dm} of dark matter for the former, while mass and annihilation cross section for the latter. (For annihilation case, dark matter clustering is another factor to determine the gamma-ray signals.) First, we mainly focus on decaying scenarios. Sec. 2.1 discusses possible final states of decaying dark matter that can explain the AMS-02 excesses. In Sec. 2.2 the EGRB from decaying dark matter is given. We discuss the annihilating scenarios at the end of each section.

¹The electroweak correction, which is not included in our study, gets important for TeV mass region and might give more stringent constraints [18]. Our main goal in the current study is to show the importance of the IC process.

Final state	AMS-02 e^+ region	AMS-02 \bar{p} region	γ_{pr}	γ_{fsr}	γ_{ic}	Data
$b\bar{b}, W^+W^-$	–	excluded [16, 17]	✓	✓	no	[24]
$W^\pm l_i^\mp$ [20]	–	partly excluded [14]	✓	no	✓	[15]
$\nu\tau^\pm l_k^\mp$ [22]	partly excluded [14]	–	✓	no	✓	[15]
$\nu l_j^\pm l_k^\mp$ [22]	partly excluded [14]	–	–	no	✓	[15]
$\mu^+\mu^-$	excluded [23]	–	–	no	✓	[25]

Table 1. Possible final states from decaying dark matter to explain AMS-02 positron or anti-proton and the constraints on them from the gamma ray observations. $i, k = 1, 2, 3$ for $W^\pm l_i^\mp$, $\nu\tau^\pm l_k^\mp$ and j, k are 1 or 2 for $\nu l_j^\pm l_k^\mp$. (Neutrino flavor is irrelevant, thus it is omitted.) ‘AMS-02 e^+ (\bar{p}) region’ indicates $m_{\text{dm}} \simeq 1\text{--}10$ TeV and $\tau_{\text{dm}} \simeq 10^{26}\text{--}10^{27}$ s, which is shown to explain the observed positron (anti-proton) excesses, and ‘–’ in their column means there is no explicit study for the latest positron (anti-proton) data. ✓ in γ_{pr} , γ_{fsr} , γ_{ic} (gamma rays produced primarily, via final state radiation, via inverse-Compton process, respectively) columns indicates gamma rays from dark matter which are computed to constrain the scenarios. For $b\bar{b}, W^+W^-$, for example, gamma rays produced primarily from the decay and final state radiation are taken into account, but gamma rays from inverse-Compton scattering are not. ‘–’ in γ_{pr} shows that there is no primary gamma rays. Final column shows the data used to give constrains in each study of refs. [14, 16, 17, 23].

2.1 Scenarios of (decaying) dark matter

Scenarios of decaying dark matter are classified by the final state of the decay process, *i.e.*, the final state contains (a) hadrons, (b) hadrons and leptons, and (c) leptons. (Here lepton means electron/positron or muon.) In the later discussion, we sometimes refer to the scenarios (a), (b), and (c) as hadronic, hadroleptonic, and leptonic scenarios (or final states), respectively. Obviously the final state needs to have leptons and hadrons in order to explain the observed positron and anti-proton excesses, respectively.

In decaying dark matter scenarios, $m_{\text{dm}} \simeq 1\text{--}10$ TeV and $\tau_{\text{dm}} \simeq 10^{26}\text{--}10^{27}$ s (roughly on $m_{\text{dm}}\tau_{\text{dm}} \simeq 10^{27}$ TeV s line) gives a good fit for the anti-proton excess and the positron excess reported by AMS-02. As a concrete model, ref. [20] studied decaying gravitino dark matter via $L_i H_u$ -type R_p -violated supersymmetric model for the anti-proton excess. It is known that the main decay mode of gravitino decay under $L_i H_u$ -type R_p -violation is $W^\pm l^\mp$ [21], which corresponds to the hadroleptonic case. On the other hand, ref. [22] considers decaying wino dark matter in $L_i L_j E_k^c$ -type R_p -violation to show that the decay can explain the positron flux. In this case, the decay products are leptons, *i.e.*, $\nu l^\pm l^\mp$, leptonic final state (or hadroleptonic final state when $l = \tau$).

Table 1 summarizes the current status of decaying dark matter that can explain the anomalous fluxes. In hadronic scenarios, such as $b\bar{b}, W^+W^-$, lots of high energy gamma rays are produced primarily from the dark matter decay, which is mainly from π^0 decay after hadronization. In addition, it has been recently realized that the cross correlation between the extragalactic gamma rays from dark matter and the observed galaxy catalog gives severe constraints on both annihilating and decaying dark matter scenarios. It is easy to read from refs. [16, 17, 20] that the parameter region which is suitable for the positron or anti-proton excesses is already excluded for final state $b\bar{b}, W^+W^-$. For $\mu^+\mu^-$ final state, on the other hand, there is no primary gamma rays from the final state. However, it was pointed out that electrons and positron from muons create high energy gamma rays by scattering off the CMB photon, *i.e.* inverse-Compton scattering, even in extragalactic region [12]. These gamma

rays are calculated with little theoretical uncertainty, thus it can give robust constraints on decaying dark matter scenarios. As the result, it was shown that leptonic scenarios, such as $\mu^+\mu^-$ final state, to account for the positron excess were already excluded [23] by Fermi-LAT 2010 data [25]. This is basically due to the fact that the spectrum of produced e^\pm is very hard and yields large amount of the IC gamma rays. Therefore, remaining possibility for the decaying scenarios suitable for the cosmic ray excesses are hadroleptonic final states, *e.g.*, $W^\pm l_i^\mp$, or three-body leptonic final state, *e.g.*, $\nu l_j^\pm l_k^\mp$. (i, j, k are flavor indices and we omit flavor index for neutrino since it is irrelevant in our discussion. We do not distinguish neutrino and anti-neutrino for the same reason.) In these cases, produced e^\pm are softer compared to $\mu^+\mu^-$ or e^+e^- final states. Thus the constraints from the gamma-ray observations are weaker.

In the present work we extend the past analysis to further constrain the decaying dark matter scenario. We use cross correlation of gamma rays from dark matter with galaxy catalogs to constrain the dark matter scenarios. In the calculation of the gamma rays from dark matter we take into account all contributions, *i.e.*, gamma rays produced primarily, via final state radiation, and via IC process. Namely, in the language of Table 1, our strategy is expressed by all \checkmark marks for γ_{pr} , γ_{fsr} , γ_{ic} , and to adopt cross-correlating technique using the galaxy catalog data [24]. Although our main target is to study the final state such as $W^\pm l_i^\mp$ or $\nu l_j^\pm l_k^\mp$ motivated by the AMS-02 excesses, we analyze the other final states, such as $b\bar{b}$, W^+W^- , $l_i^+l_i^-$, to give constraints for general use.

The final state does not depend on its origin, decay or annihilation.² Thus the discussion here can also cover the annihilation case. Typical examples are $b\bar{b}$, W^+W^- , and $l_i^+l_i^-$.

2.2 Gamma rays from dark matter

As described at the beginning of this section, the spectrum of gamma rays is determined by three components, the dark matter mass m_{dm} and lifetime τ_{dm} , and the decaying scenario, *i.e.*, final state of the decay process. When the final states are specified, the energy distributions dN_I/dE of the decay products $I = \gamma, e^\pm$, etc., are determined.

We derive the ‘window function’, which is needed for the calculation of both the gamma-ray intensity and the angular cross correlation between gamma rays from dark matter and galaxy catalogs. We start with defining the gamma-ray intensity from decaying dark matter:

$$\frac{d\Phi_\gamma^{\text{dm}}}{d\chi}(E_\gamma, z) = \frac{1}{4\pi} \frac{\Omega_{\text{dm}}\rho_c}{m_{\text{dm}}\tau_{\text{dm}}} \frac{1}{1+z} Q_\gamma^{\text{dm}}(E'_\gamma, z) e^{-\tau(E'_\gamma, z)}. \quad (2.1)$$

χ is comoving distance, E_γ is the energy of a gamma ray which we observe today, and E'_γ is the gamma-ray energy at the redshift z , *i.e.*, $E'_\gamma = (1+z)E_\gamma$. $\tau(E'_\gamma, z)$ is the optical depth, for which we will use data given in ref. [26]. $Q_\gamma^{\text{dm}}(E'_\gamma, z)$ is a gamma-ray source function due to dark matter, given as

$$Q_\gamma^{\text{dm}}(E'_\gamma, z) = Q_{\gamma_{\text{pr}}}^{\text{dm}}(E'_\gamma, z) + Q_{\gamma_{\text{fsr}}}^{\text{dm}}(E'_\gamma, z) + Q_{\gamma_{\text{ic}}}^{\text{dm}}(E'_\gamma, z), \quad (2.2)$$

where

$$Q_{\gamma_{\text{pr}}}^{\text{dm}}(E'_\gamma, z) + Q_{\gamma_{\text{fsr}}}^{\text{dm}}(E'_\gamma, z) = (1+z) \frac{dN_\gamma}{dE}(E'_\gamma), \quad (2.3)$$

$$Q_{\gamma_{\text{ic}}}^{\text{dm}}(E'_\gamma, z) = c \int dE_e dE_{\gamma_{\text{BG}}} (1+z) \frac{d\sigma_{\text{IC}}}{dE'_\gamma}(E'_\gamma, E_e, E_{\gamma_{\text{BG}}}) f_\gamma^{\text{BG}}(E_{\gamma_{\text{BG}}}, z) \frac{Y_e(E_e)}{b_{\text{IC}}(E_e, z)}. \quad (2.4)$$

²Of course, final states $W^\pm l_i^\mp$, $\nu l_j^\pm l_k^\mp$ are impossible for annihilation case.

c is the speed of light. The former describes the gamma-ray source primarily produced by the dark matter decay. dN_γ/dE is the energy distribution of primary gamma rays from single dark matter decay, including final state radiation (FSR) photons. For the computation, we use PYTHIA 6.4 [27] (not including the electroweak corrections).³ The latter represents the IC scattering between e^\pm from dark matter and the background photons. $d\sigma_{\text{IC}}/dE'_\gamma$ is the differential cross section of the IC process. $f_\gamma^{\text{BG}}(E_{\gamma\text{BG}}, z)$ is the energy spectrum of the background photon field (in unit energy and volume). In our study we take into account both the CMB and extragalactic background light (EBL) photons, *i.e.*,

$$f_\gamma^{\text{BG}}(E_{\gamma\text{BG}}, z) = f_\gamma^{\text{CMB}}(E_{\gamma\text{BG}}, z) + f_\gamma^{\text{EBL}}(E_{\gamma\text{BG}}, z). \quad (2.5)$$

For the EBL, we will use the spectrum given in ref. [26]. $Y_e(E_e)$ is defined as

$$Y_e(E_e) = \sum_{I=e^\pm} \int_{E_e}^{\infty} dE \frac{dN_I}{dE}(E), \quad (2.6)$$

where dN_{e^\pm}/dE is the e^\pm energy distribution from dark matter. Finally $b_{\text{IC}}(E_e, z)$ is the energy loss rate (per unit time) of e^\pm with energy E_e , which is given by

$$b_{\text{IC}}(E_e, z) = \int dE'_\gamma dE_{\gamma\text{BG}} (E'_\gamma - E_{\gamma\text{BG}}) \frac{d\sigma_{\text{IC}}}{dE'_\gamma}(E'_\gamma, E_e, E_{\gamma\text{BG}}) f_\gamma^{\text{BG}}(E_{\gamma\text{BG}}, z) \quad (2.7)$$

$$\equiv b_{\text{IC}}^{\text{CMB}}(E_e, z) + b_{\text{IC}}^{\text{EBL}}(E_e, z), \quad (2.8)$$

where the first and second terms of the right-hand side in the second line are the energy loss rates due to the CMB and EBL, respectively. Under the CMB, the energy loss rate well agrees with an analytic expression $b_{\text{IC},T}^{\text{CMB}}(E_e, z) = (1+z)^4 (4/3) \sigma_T (E_e/m_e)^2 \rho_{\text{CMB}}^{(\text{now})}$ (σ_T , m_e are Thomson scattering cross section, electron mass, respectively, and $\rho_{\text{CMB}}^{(\text{now})} \simeq 0.260 \text{ eV cm}^{-3}$), especially for $E_e \lesssim 1 \text{ TeV}$.⁴ However, for e^\pm with $E_e \gtrsim 1 \text{ TeV}$, the energy loss rate deviates from the analytic expression. This is because it is given in the Thomson limit where the background photon energy is much smaller than the incident electron energy (or electron mass in the electron rest frame). (See Fig. 11 in Appendix.) In addition, we have checked that the energy loss due to the EBL photon is much smaller than one due to the CMB, *e.g.*, it accounts for just around 5% in the total energy loss rate for $z = 0$ and smaller for higher z . This is because the intensity of the EBL is much smaller than the CMB. Thus, the energy loss rate of e^\pm can be computed with little theoretical uncertainty since it is determined mainly by the CMB.

In Fig. 1, we show the gamma-ray intensity $d\Phi_\gamma^{\text{dm}}/d\chi(E_\gamma, z)$ from decaying dark matter. Here final states of the decay are $\nu\mu^\pm e^\mp$ and $\nu e^\pm e^\mp$ (which corresponds to $L_1 L_2 E_1^c$ -type R_p violation) and $W^\pm \mu^\mp$, and the results for redshift $z = 0, 1$ and 5 are shown. For each z the total gamma-ray intensity (solid) and one without IC gamma ray (dashed) are plotted. The

³The FSR is important especially for leptonic final state. While we ignored the FSR in our previous study [14], we have checked that inclusion of FSR only give minor changes for hadronic and hadroleptonic scenarios. For leptonic case, on the other hand, we have found that the constraints become tighter for $m_{\text{dm}} \lesssim 1 \text{ TeV}$.

⁴Using the analytic expression for f_γ^{CMB} and $b_{\text{IC}}^{\text{CMB}}$ and neglecting the EBL, $Q_{\gamma,\text{IC}}^{\text{dm}}(E'_\gamma, z)$ agrees with $(1+z)\mathcal{P}_{\text{ic}}(E'_\gamma)$ in eq. (2.5) of ref. [14]. In this equation $d\sigma_{\text{IC}}/dE'_\gamma(E'_\gamma, E_e, E_{\gamma\text{CMB}})$ should be replaced by $d\sigma_{\text{IC}}/dE'_\gamma(E'_\gamma, E_e, (1+z)E_{\gamma\text{CMB}})$. Similarly, $\tau(z, E_\gamma)$ should be $\tau(z, E'_\gamma)$ in eq. (2.3) of ref. [14]. Those are just typos, and the numerical calculation had been done in the correct expressions.

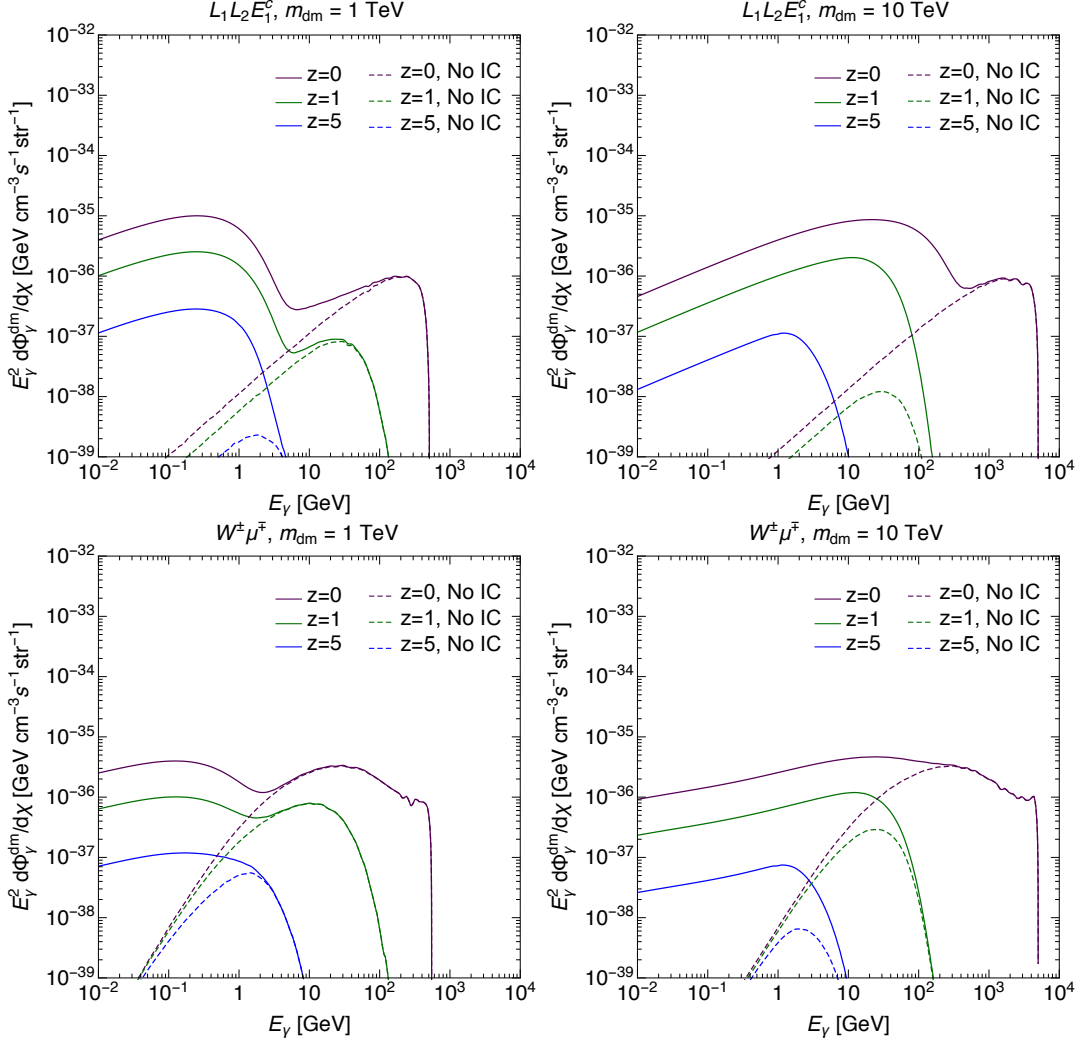


Figure 1. Gamma-ray intensity $d\Phi_{\gamma}^{\text{dm}}/d\chi(E_{\gamma}, z)$ from decaying dark matter. Results are shown for $\nu\mu^{\pm}e^{\mp}$ and $\nu e^{\pm}e^{\mp}$ and $W^{\pm}\mu^{\mp}$ final states. Total (without IC contribution) intensities for $z = 0, 1, 5$ from top to bottom are plotted in solid (dashed) lines. Dark matter mass is taken as 1 (left) and 10 (right) TeV.

intensity agrees with rough estimation from eq. (2.1):

$$\begin{aligned}
 E_{\gamma}^2 \frac{d\Phi_{\gamma}^{\text{dm}}}{d\chi}(E_{\gamma}, z) &\simeq 9.9 \times 10^{-36} \text{ GeV cm}^{-3} \text{ s}^{-1} \frac{10^{27} \text{ TeV s}}{m_{\text{dm}} \tau_{\text{dm}}} \left(\frac{E_{\gamma}}{1 \text{ GeV}} \right)^2 \\
 &\times \frac{1}{1+z} \left[10 \text{ MeV } Q_{\gamma}^{\text{dm}}(E'_{\gamma}, z) \right] e^{-\tau(E'_{\gamma}, z)}. \quad (2.9)
 \end{aligned}$$

Here we have estimated $Q_{\gamma}^{\text{dm}} \sim Q_{\gamma_{\text{ic}}}^{\text{dm}} \sim 1/(10 \text{ MeV})$ in the Thomson limit. This is based on the fact that in the Thomson limit the maximum energy of scattered photon due to electron with an energy of $\sim \text{TeV}$ in the CMB is $\sim \text{GeV}$ and the energy distribution of the scattered photon is peaked at lower energy. For $\nu\mu^{\pm}e^{\mp}$ and $\nu e^{\pm}e^{\mp}$ final state, a peak in high-energy regions comes from the FSR while another peak in lower energy corresponds to the

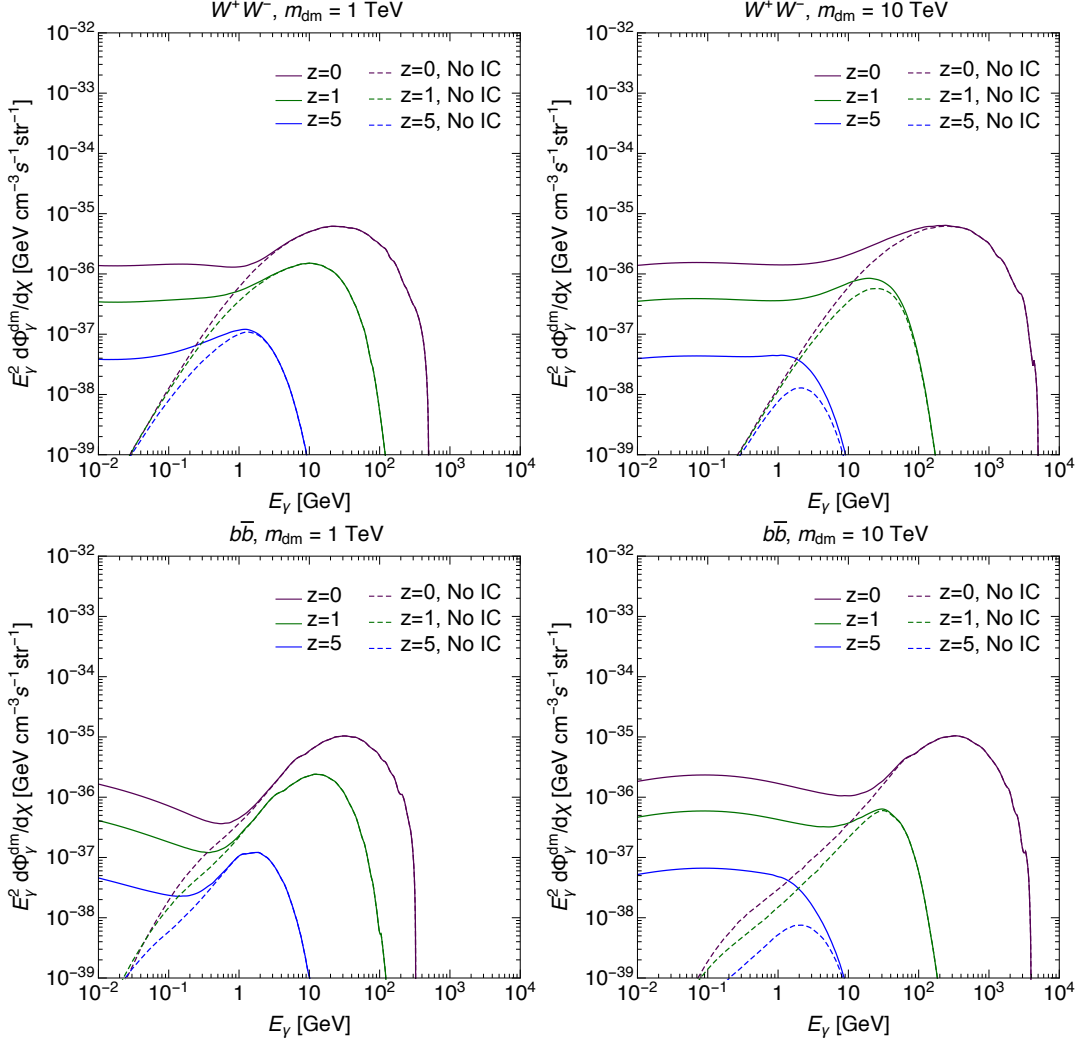


Figure 2. Same as Fig. 1 but for W^+W^- and $b\bar{b}$ final states.

IC gamma rays. Although its energy range is lower, it is clear that the intensity of the IC gamma rays is much larger than that of the FSR. For $W^\pm\mu^\mp$ case, the first peak in high energy region is mainly the contribution from the primary decay. The FSR is subdominant, which can be seen by comparing the result of W^+W^- final state in Fig. 2. (In the figure the same results but for $b\bar{b}$ final states is shown too.) The comparison with W^+W^- also gives us the importance of the IC gamma rays in lower energy region. The IC gamma rays in $W^\pm\mu^\mp$ mainly attributes to e^\pm from μ^\pm .

Eventually we get the window function

$$W_\gamma^{\text{dm}}(z) = \int_{E_{\text{min}}}^{E_{\text{max}}} dE_\gamma \frac{d\Phi_\gamma^{\text{dm}}}{d\chi}(E_\gamma, z). \quad (2.10)$$

E_{max} and E_{min} shows the energy region of gamma rays we compute for the cross correlation with galaxy catalog. (See Sec. 4.) It is obvious from eqs. (2.1)–(2.10) that the window function can be obtained with little uncertainty if we specify dN_I/dE , m_{dm} and τ_{dm} . This is not

exactly the same for annihilation. In annihilation, although the window function is given similarly to the decaying case, just by replacing the gamma-ray intensity eq. (2.1) to

$$\frac{d\Phi_\gamma^{\text{dm}}}{d\chi}(E_\gamma, z)|_{\text{ann}} = \frac{1}{8\pi} \frac{\langle\sigma v\rangle(\Omega_{\text{dm}}\rho_c)^2}{m_{\text{dm}}^2} (1+z)^3 Q_\gamma^{\text{dm}}(E'_\gamma, z) \langle(1+\delta)^2\rangle e^{-\tau(E'_\gamma, z)} \quad (2.11)$$

$$\simeq 6.2 \times 10^{-43} \text{ GeV}^{-1} \text{ cm}^{-3} \text{ s}^{-1} \frac{\langle\sigma v\rangle}{10^{-25} \text{ cm}^3 \text{ s}^{-1}} \left(\frac{1 \text{ TeV}}{m_{\text{dm}}}\right)^2 \times (1+z)^3 \left[10 \text{ MeV } Q_\gamma^{\text{dm}}(E'_\gamma, z)\right] \langle(1+\delta)^2\rangle e^{-\tau(E'_\gamma, z)}, \quad (2.12)$$

where $\langle\sigma v\rangle$ is annihilation cross section, an extra factor $\langle(1+\delta)^2\rangle$, where the dark matter overdensity $\delta = (\rho_{\text{dm}} - \langle\rho_{\text{dm}}\rangle)/\langle\rho_{\text{dm}}\rangle$ (ρ_{dm} is energy density of dark matter), is needed to give gamma rays in line-of-sight. This factor boosts the annihilation rate, giving rise to much larger gamma-ray intensity. However, it is accompanied with an uncertainty related to how one simulates clustering of (dark) matter and extrapolates the results down to sub-grid scales. We note that recent theoretical studies (*e.g.*, ref. [28]) discuss how to reduce the uncertainty to have a better handle on the clustering properties. (See discussion in Sec. 5.1.)

3 Extragalactic gamma-ray background from astrophysical sources

As in our previous paper [14], we considered two astrophysical sources as a potential contaminating background for dark matter searches; blazars and star-forming galaxies.

Blazars are the dominant gamma-ray source, thousands of which have been detected with Fermi-LAT [29]. Their number densities per unit luminosity range (*i.e.*, the luminosity function dn_γ/dL_γ) have been constructed by using the luminosity-dependent density evolution model [30]. They are characterized by a double-power-law function, where the break luminosity depends on redshift. The window function $W_\gamma(z)$ is then computed as

$$W_\gamma^X(z) = \chi^2 \int dL_\gamma \frac{dn_\gamma^X(L_\gamma, z)}{dL_\gamma} F_\gamma(L_\gamma, z), \quad (3.1)$$

where the superscript X represents astrophysical sources: blazars and star-forming galaxies, $F_\gamma = L_\gamma/[4\pi(1+z)\chi^2]$ is the number flux of the gamma-ray photons from a source with the luminosity L_γ and at the redshift z . With the most recent luminosity function, ref. [30] showed that the blazar component could explain about 50% of the gamma-ray background above 100 MeV, while most above 100 GeV.

At low energies, there are softer astrophysical components playing a major role in the gamma-ray intensity. One such class is the star-forming and starburst galaxies, where cosmic rays supplied by supernovae produce gamma rays from interactions with interstellar medium. There is an established correlation between the gamma-ray luminosity and infrared luminosity, which is a proxy for star-formation activity [31]. Combining this with recent measurements of the infrared luminosity function [32], ref. [33] obtained the gamma-ray luminosity function for both the star-forming and starburst galaxies. One can then compute the window function for these galaxies by using eq. (3.1). They can give significant contribution to the gamma-ray background, particularly at low energies. A similar contribution is also expected from another gamma-ray source class: misaligned active galactic nuclei [34, 35]. We do not, however, include this population in our analysis, as their contribution to the gamma-ray

background is similar to that from the star-forming galaxies, but with larger uncertainties. Including it will further constrain the parameter spaces of dark matter.

The astrophysical contributions from all these sources can accommodate most (if not all) of the measured energy spectrum of the EGRB. See Fig. 9 of ref. [36] for a summary plot. Therefore, one can obtain stringent constraints on both dark matter decay [14] and annihilation [30, 37] from the energy spectrum alone. One can further tighten these limits by investigating clustering properties of the gamma-ray data, *e.g.*, by cross-correlating with galaxy distributions, as we shall discuss in the following sections.

4 Cross correlation between the extragalactic gamma-ray background with galaxy catalogs

Galaxies trace underlying dark matter distribution, and therefore, it is expected that the distribution of the gamma-ray photons that come from dark matter decay or annihilation are spatially correlated with those of galaxies. This cross correlation between gamma-ray emitters (γ) and galaxies (g) is quantified by the angular cross-power spectrum as

$$C_\ell^{\gamma g} = \int \frac{d\chi}{\chi^2} W_\gamma(z) W_g(z) P_{\gamma g} \left(k = \frac{\ell}{\chi}, z \right), \quad (4.1)$$

where $W_g(z)$ is related to the redshift distribution of galaxies in a catalog through $W_g = (d \ln N_g / dz)(dz / d\chi)$. $P_{\gamma g}(k, z)$ is the cross-power spectrum between the gamma-ray sources and galaxies at wave number k and redshift z . For discussions of decaying dark matter and astrophysical sources, we assume that it is well approximated by a matter power spectrum with a constant bias parameter: $P_{\gamma g}(k, z) \approx b_\gamma b_g P_m(k, z)$ (P_m is matter power spectrum), and $b_{\text{dm}} = 1$ for the dark matter component. (See later discussion for b_g .) For annihilating dark matter, on the other hand, since the rate of annihilation depends on the density squared, one has to evaluate the cross-power spectrum between the density squared and density, $P_{\delta^2 \delta}(k, z)$, and we assume $P_{\gamma g}(k, z) \approx b_g P_{\delta^2 \delta}(k, z)$. For computing $P_{\delta^2 \delta}(k, z)$, we follow an analytic halo-model prescription introduced in ref. [38].

A great advantage of taking cross correlation over analyzing the energy spectrum of the gamma-ray background is that one can filter gamma-ray emission from a preferred redshift range. This can be seen from the fact that the integrand of eq. (4.1) depends on $W_\gamma(z)W_g(z)$, because distribution of gamma-ray sources are uncorrelated with galaxy distribution at different redshifts. Since larger contributions from dark matter annihilation and decay come from lower redshift, while it is opposite for ordinary astrophysical sources [39], one can efficiently remove the astrophysical backgrounds by choosing galaxy catalogs. Several theoretical studies showed that the sensitivity for dark matter from the cross correlation would be much tighter than that from the energy spectrum [38–40].

Recently, ref. [24] measured cross correlations between the gamma-ray background measured with Fermi-LAT with several galaxy catalogs. The catalogs that the authors used for the analyses are SDSS QSO, 2MASS, NVSS, SDSS MG, and SDSS LRG, and they found positive signatures at greater than 3.5σ for the first three catalogs, and about 3σ for the last two. Particularly, the 2MASS catalog is for the lowest-redshift galaxies, which peak around $z \sim 0.1$, which is the most suitable for dark matter searches. The cross-correlation measurements are then interpreted and used to put constraints on dark matter properties as well as astrophysical models. By conservatively including dark matter alone, ref. [16] showed

that the lower limits on, *e.g.*, decay lifetime of dark matter, were quite stringent, being improved by about one order of magnitude compared with the previous limits obtained with the spectral analysis [14]. Reference [17] extended the analyses to include a few astrophysical components, and showed that the limits further improved by factors of several.

In this paper, we consider both decaying (or annihilating) dark matter component and two classes of astrophysical sources (blazars and star-forming galaxies). For the cross-power spectrum $P_{\gamma g}$, we assume that biases of the astrophysical sources (b_γ) are both 1. This is conservative because typical astrophysical sources are considered and that they are found to be positively biased (*i.e.*, $b_\gamma > 1$) [41]. For the bias parameter of galaxies in the chosen catalogs (b_g), we adopt the values found in ref. [24]. In addition to these ‘source’ terms for $C_\ell^{\gamma g}$, we also include a noise term, constant as a function of ℓ . This is to accommodate the shot-noise term that comes from the fact that the astrophysical sources are point-like sources, and hence, it yields such a scale-independent term in the power spectrum [39]. It is also meant to correct for uncertainties of the power spectrum at small angular scales, as also mentioned in ref. [17]. For these correction terms, we follow the prescription in ref. [17], where $C_{\text{corr}}^{\gamma g} = A_{\gamma g}$, and they are function of both gamma-ray energy (γ) and galaxy catalog (g). But we assume that the energy spectrum is represented as $E^{-2.3}$ that is the measured EGRB spectrum, which leaves five independent parameters A_g for > 1 GeV, corresponding to five galaxy catalogs ($g = \{\text{QSO}, 2\text{MASS}, \text{NVSS}, \text{MG}, \text{LRG}\}$).

5 Results

5.1 Analysis including dark matter component alone

First we perform a conservative analysis by taking dark matter component only into account. We use the data for the angular cross-power spectrum $C_\ell^{\gamma g}$ for gamma-ray data in three energy bins (> 500 MeV, > 1 GeV, and > 10 GeV) and five different galaxy catalogs, as obtained in ref. [24]. For a given dark matter mass and a final state, we compute a χ^2 statistic:

$$\chi^2 = \sum_{\gamma, g} \sum_{\ell, \ell'} (C_{\text{dat}}^{\gamma g} - C_{\text{th}}^{\gamma g})_\ell (\text{Cov}^{-1})_{\ell \ell'} (C_{\text{dat}}^{\gamma g} - C_{\text{th}}^{\gamma g})_{\ell'}, \quad (5.1)$$

in order to obtain a constraint on τ_{dm} ($\langle \sigma v \rangle$) for decay (annihilation) scenario.⁵ Here ‘dat’ and ‘th’ represent data and theoretical value, respectively, ‘Cov’ is the covariance matrix for the cross-correlation measurements, and γ and g run for three energy and five galaxy bins, respectively. After obtaining the minimum χ^2 by solving $\partial \chi^2 / \partial \tau_{\text{dm}} = 0$ or $\partial \chi^2 / \partial \langle \sigma v \rangle = 0$, we solve $\Delta \chi^2 \equiv \chi^2 - \chi_{\text{min}}^2 = 2.71$ in order to obtain the 95% confidence level limit on τ_{dm} or $\langle \sigma v \rangle$.

In Figs. 3–5, we show 95% confidence level lower limits on the decay lifetime for various decay modes. We also show the effect of including the IC scattering off both the CMB and EBL photons in the analysis. In fact it is found that the IC scattering is very important for the decay channels that involve leptons in the final state and for dark matter heavier than ~ 1 TeV. This is clearly seen in Figs. 3 and 4. The constraints due to the IC process have improved the lower limits by more than one order of magnitude for TeV region. The limits are better than those given from clusters or dwarf galaxies. For example, in $\mu^+ \mu^-$ channel, our result shows that $\tau_{\text{dm}} \lesssim (3\text{--}10) \times 10^{26}$ sec for $m_{\text{dm}} = 1\text{--}10$ TeV. This is more stringent limit by a factor of a few compared to the latest constraints from dwarf galaxies [42]. (See

⁵This χ^2 has nothing to do with the comoving distance, although the same symbol χ is used.

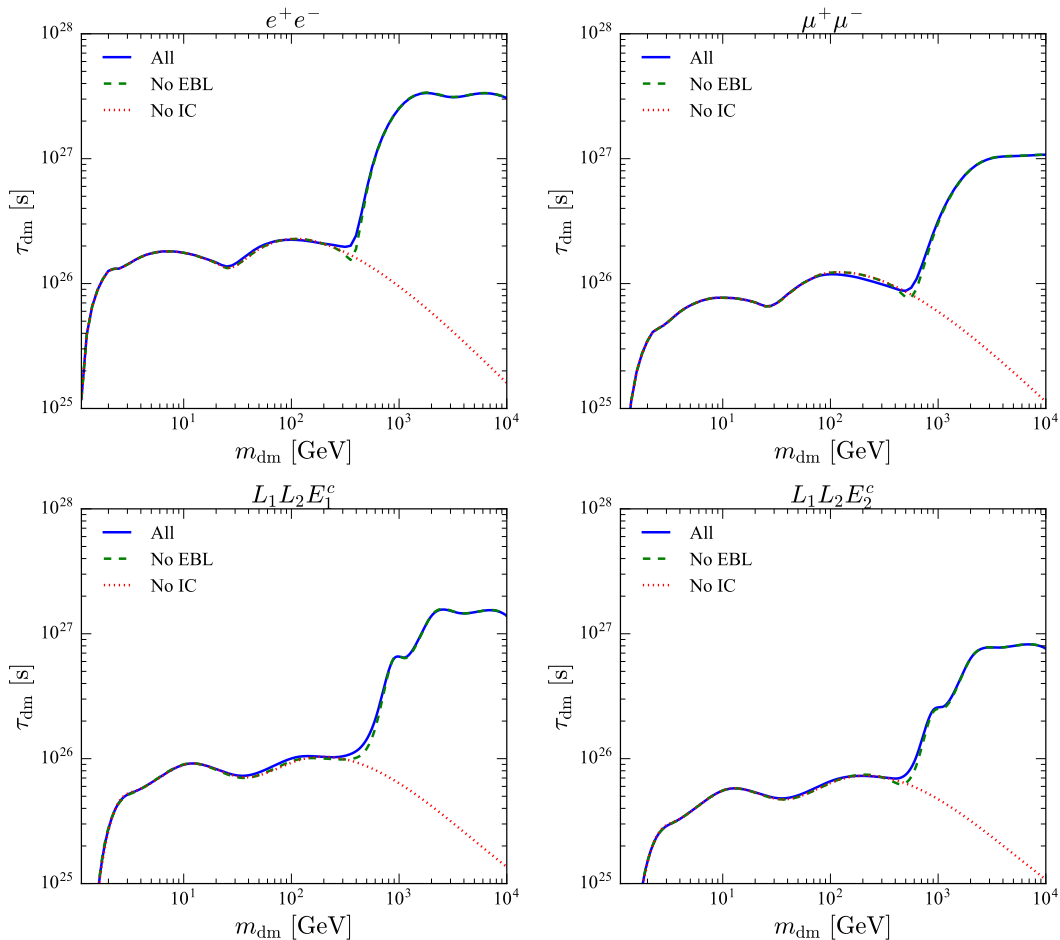


Figure 3. Lower limits on dark matter lifetime for leptonic channels due to cross correlation between the gamma-ray background and five galaxy catalogs. In this analysis, only dark matter component is included. IC scattering off both the EBL and CMB photons are included in solid, only CMB in dashed, and no IC effect is included in dotted.

also related past works [43, 44].) We note that our results for no-IC case well agree with those of ref. [16].

Let us see the scenarios motivated to explain the AMS-02 positron excess. As discussed in Sec. 2.1, three-body leptonic decay gives a good fit to explain the positron excess. The numerical results for $L_i L_j E_k^c$ in Figs. 3 and 4 correspond to the final state $\nu_i e_j^\pm e_k^\mp$ & $\nu_j e_i^\pm e_k^\mp$. It is seen that $\tau_{\text{dm}} \lesssim 10^{27}$ s is excluded for $m_{\text{dm}} \gtrsim 1$ TeV in cases of $L_1 L_2 E_1^c$ and $L_1 L_2 E_2^c$. These constraints exclude part of preferred region to explain the positron excess [22]. Similarly, the preferred parameter spaces are partly excluded for $L_1 L_2 E_3^c$ and $L_3 L_2 E_3^c$.

We have drawn a similar conclusion for the scenario to explain the AMS-02 anti-proton excess, *i.e.*, the preferred region in $W^\pm \mu^\mp$ scenario [20] is partly excluded. It is well-known that there is a huge uncertainty in the calculation of cosmic-ray (anti-)protons. This uncertainty can be estimated by considering three propagation models, MIN, MED and MAX [45]. Reading from the result in ref. [20], one can explain the excess while satisfying the present constraint if MAX or MED models for (anti-)proton propagation are adopted. It will be

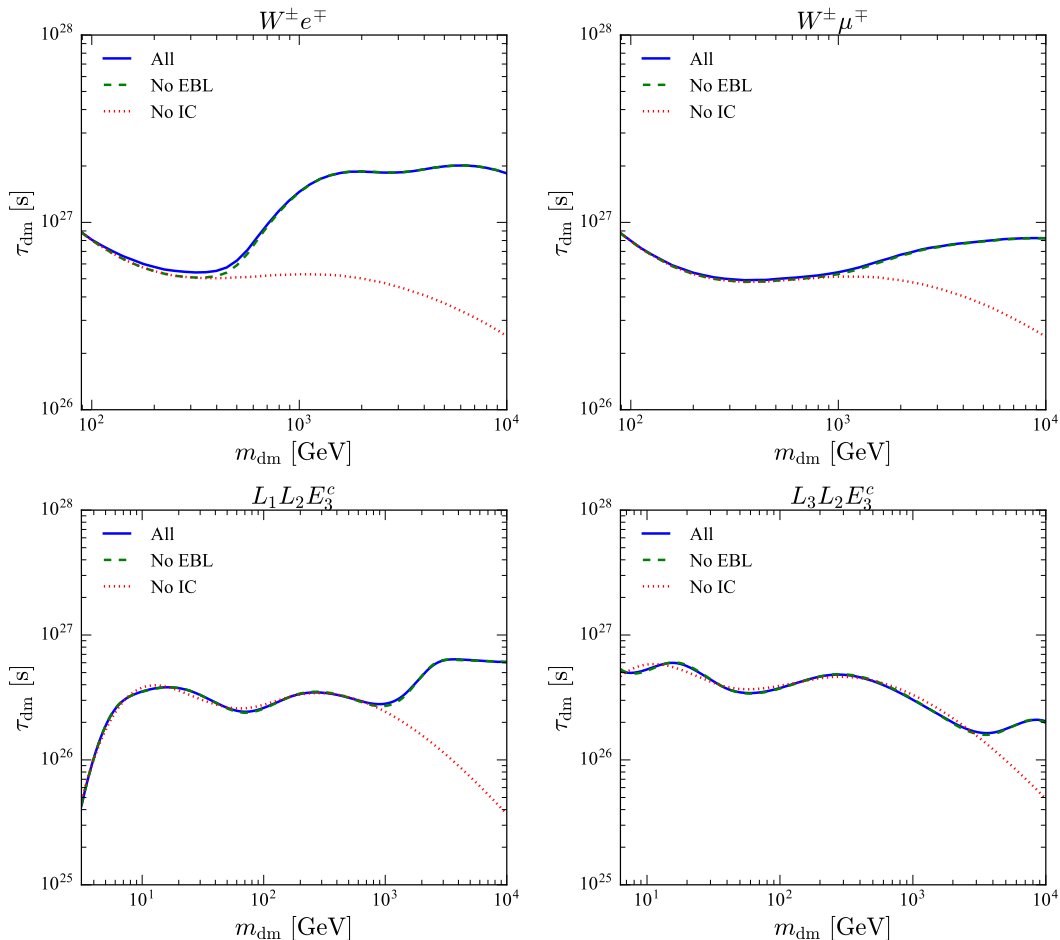


Figure 4. The same as Fig. 3 but for hadroleptonic channels.

shown in the next subsection, however, that the remaining parameter regions for $L_i L_j E_k^c$ and $W^\pm \mu^\mp$ final states are excluded when the astrophysical components are taken into account.

In Figs. 3 and 4, we also show the results for the decay channels which are not suitable for the explanation of these excesses. Those are for readers who are interested in the decay channels in different context. Figure 5, which shows the results for hadronic channels, is for the same purpose. For hadronic channels the impact of the IC process is small. This is expected since there are fewer energetic electrons and positrons in the cascading products.

Two more remarks are in order. First, including the EBL photons has little impact on the total IC results, since their energy density is much smaller than that of the CMB photons. This is expected from the discussion given in Sec. 2.2. Therefore, we conclude that our results presented in these figures are robust constraints on decaying dark matter. Second, the obtained constraints are much stronger than those in the previous studies, especially in the TeV mass region for leptonic and hadroleptonic channels. In ref. [14], the gamma-ray background *spectrum* is used to constrain the decaying dark matter. (Here the IC process is considered.) Figure 6 in the reference, which is obtained by including only dark matter

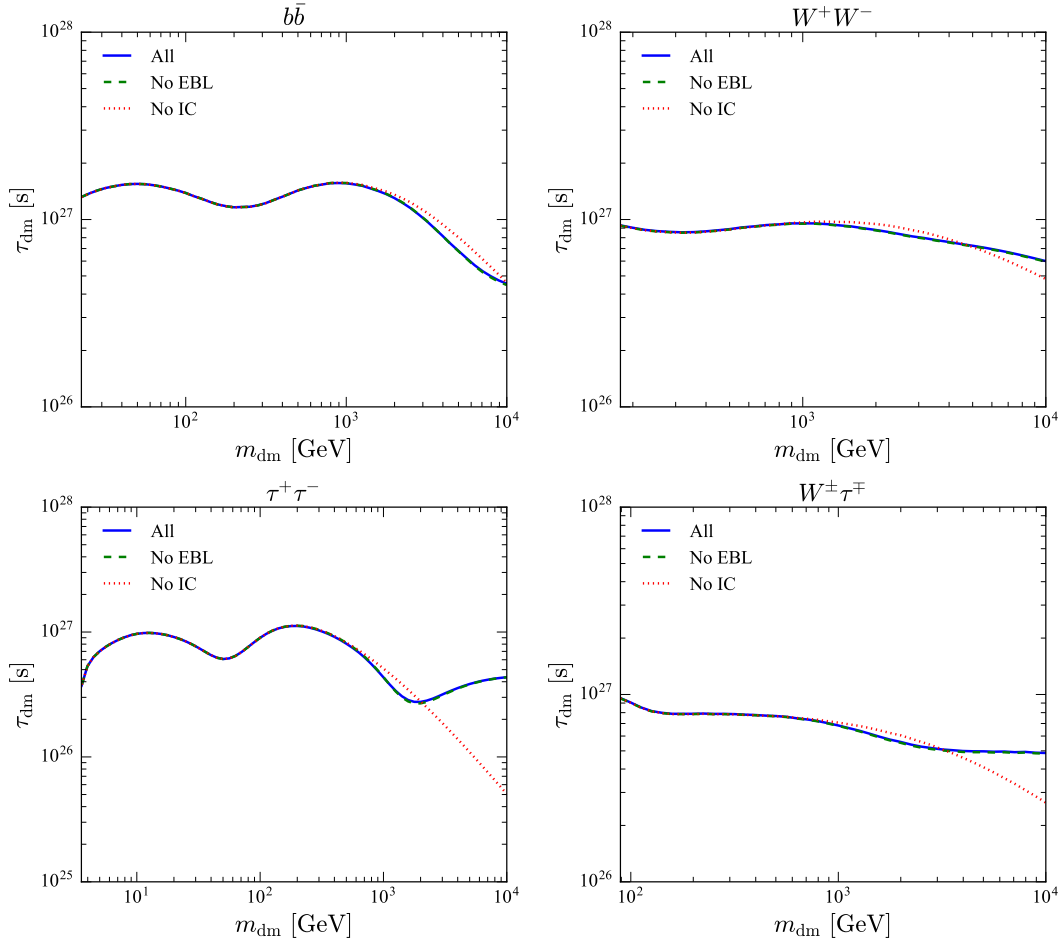


Figure 5. The same as Fig. 3 but for the hadronic channels.

contribution, shows that $\tau_{\text{dm}} \lesssim 10^{26}$ s is excluded for $m_{\text{dm}} \gtrsim 1$ TeV. Similar constraints are obtained by ref. [16] using the *cross-correlation* technique but the IC process is ignored. Thus, these two facts show that analysis of the angular cross-correlation of the gamma-ray background by taking the IC effect into account is important for the investigation on dark matter scenarios.

Finally we did the same analysis for annihilating scenarios, e^+e^- , $\mu^+\mu^-$, $b\bar{b}$, W^+W^- , and $\tau^+\tau^-$. Upper limits on $\langle\sigma v\rangle$ at 95% confidence level are shown in Fig. 6. Compared to the decaying case, the computation of $P_{\delta^2\delta}(k, z)$ involves uncertainty. In the current analysis we largely followed ref. [38], except for adopting the substructure boost factor given in ref. [28]. This substructure model is based on the the latest development of the observation and simulation by taking tidal stripping and dynamical friction into account, and consequently it predicts substructure boost in between the optimistic and conservative models in the previous literature [38]. Indeed, the obtained constraints reflects this fact; ‘No IC’ lines in Fig. 6 shows a bit tighter constraints compared to ‘annLOW’ lines in Fig. 3 of ref. [16], but it is weaker compared to ‘annHIGH’ line in the same figure. The effect of IC, on the other hand, is clearly seen in the annihilation cases too. Especially for e^+e^- , $\mu^+\mu^-$, the constraints

$\log(\tau_{\text{dm}}/\text{s})$	(25, 35)
$\log(\langle\sigma v\rangle/\text{cm}^3 \text{s}^{-1})$	(−30, −20)
A_{SFG}	(0, 3)
A_{blazar}	(0, 3)
A_{QSO}	$(−0.5, 0.5) \times 10^{-12} \text{ cm}^{-2} \text{ s}^{-1}$
$A_{2\text{MASS}}$	$(−0.5, 0.5) \times 10^{-12} \text{ cm}^{-2} \text{ s}^{-1}$
A_{NVSS}	$(−0.5, 0.5) \times 10^{-11} \text{ cm}^{-2} \text{ s}^{-1}$
A_{MG}	$(−0.5, 0.5) \times 10^{-12} \text{ cm}^{-2} \text{ s}^{-1}$
A_{LRG}	$(−0.5, 0.5) \times 10^{-12} \text{ cm}^{-2} \text{ s}^{-1}$

Table 2. Ranges of flat priors for the parameters studied in MCMC.

get stronger by one to two orders of magnitude in $m_{\text{dm}} \gtrsim 1 \text{ TeV}$.

5.2 Analysis including astrophysical sources and dark matter component

Realistically, it is expected that the astrophysical sources such as blazars and star-forming galaxies also contribute to the measured cross correlations. Indeed, both the shape and the amplitude of the measurements can be well explained by these astrophysical sources [24]. Including them in the analysis will not only be realistic but also tighten the constraints on the dark matter component significantly.

Here we adopt the Bayesian statistics, where the posterior distribution of theoretical parameters $\boldsymbol{\vartheta}$ given data \mathbf{d} is obtained through the Bayes theorem:

$$P(\boldsymbol{\vartheta}|\mathbf{d}) \propto P(\boldsymbol{\vartheta})\mathcal{L}(\mathbf{d}|\boldsymbol{\vartheta}), \quad (5.2)$$

where $\mathcal{L}(\mathbf{d}|\boldsymbol{\vartheta})$ is the likelihood function and $P(\boldsymbol{\vartheta})$ is the prior distribution. The likelihood function is characterized as Gaussian: $\mathcal{L} = \exp(-\chi^2/2)$ with χ^2 defined in eq. (5.1). This time, $C_{\text{th},\ell}^\gamma$ in χ^2 depends on all the theoretical parameters $\boldsymbol{\vartheta}$.

We adopt $\boldsymbol{\vartheta} = (\tau_{\text{dm}}, A_{\text{SFG}}, A_{\text{blazar}}, A_{\text{QSO}}, A_{2\text{MASS}}, A_{\text{NVSS}}, A_{\text{MG}}, A_{\text{LRG}})$ as eight free parameters for each case with a fixed m_{dm} and decay channel. (τ_{dm} should be replaced with $\langle\sigma v\rangle$ for the annihilation case.) Here A_{SFG} and A_{blazar} are the amplitudes of the angular cross-power spectrum $C_\ell^{\gamma\text{g}}$ for these astrophysical sources, and they are normalized to 1 for our model with the canonical choice of relevant parameters as described in Sec. 3. The other parameters $\{A_{\text{QSO}}, A_{2\text{MASS}}, A_{\text{NVSS}}, A_{\text{MG}}, A_{\text{LRG}}\}$ are introduced to correct for shot-noise terms that are expected for point-like astrophysical sources as well as uncertain behaviors of $C_\ell^{\gamma\text{g}}$ at small angular scales (Sec. 4). We choose flat priors in logarithmic space for τ_{dm} and $\langle\sigma v\rangle$, and linear space for the rest, and the ranges are summarized in Table 2.

With these parameters and priors, we perform the Markov-Chain Monte Carlo (MCMC) simulations using the `MultiNest` package [46–48], and show the results in Figs. 7–9. They corresponds to the results shown in Figs. 3–5, respectively, but including the contribution from the astrophysical sources. In all the cases, the constraints get stronger by an order of magnitude compared to Figs. 3–5. The results for $b\bar{b}$ and W^+W^- well agree with ref. [17]. The constraints on $\mu^+\mu^-$ and $\tau^+\tau^-$ are also consistent for $m_{\text{dm}} \lesssim 1 \text{ TeV}$. However, more stringent constraints have been obtained in $m_{\text{dm}} \gtrsim 1 \text{ TeV}$ due to the IC process. For example, leptonic channels are constrained to $\tau_{\text{dm}} \lesssim 10^{28} \text{ sec}$ for $m_{\text{dm}} \gtrsim 1 \text{ TeV}$. Consequently, the parameter regions to explain the positron excess in $L_i L_j E_k^c$ scenario or anti-proton excess in $W^\pm \mu^\mp$ final state are excluded. For anti-proton, there is uncertainty in the computation

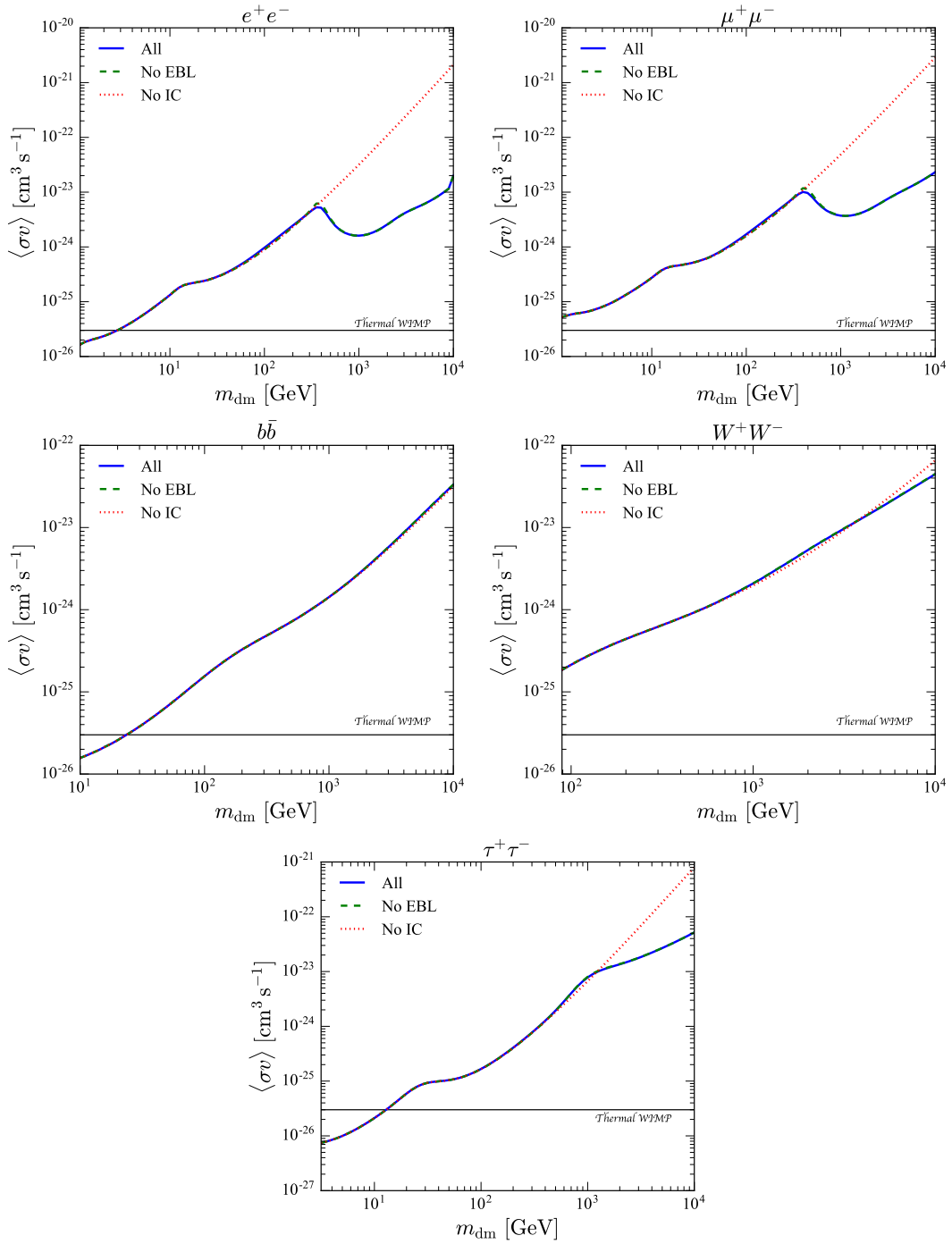


Figure 6. Upper limit on dark matter annihilation cross section $\langle\sigma v\rangle$ at 95% confidence level due to cross correlation between the gamma-ray background and five galaxy catalogs. In this analysis, only dark matter component is included. IC scattering off both the EBL and CMB photons are included in solid, only CMB in dashed, and no IC effect is included in dotted. ‘Thermal WIMP’ line shows canonical value of the cross section which is suggested in thermal WIMP scenario.

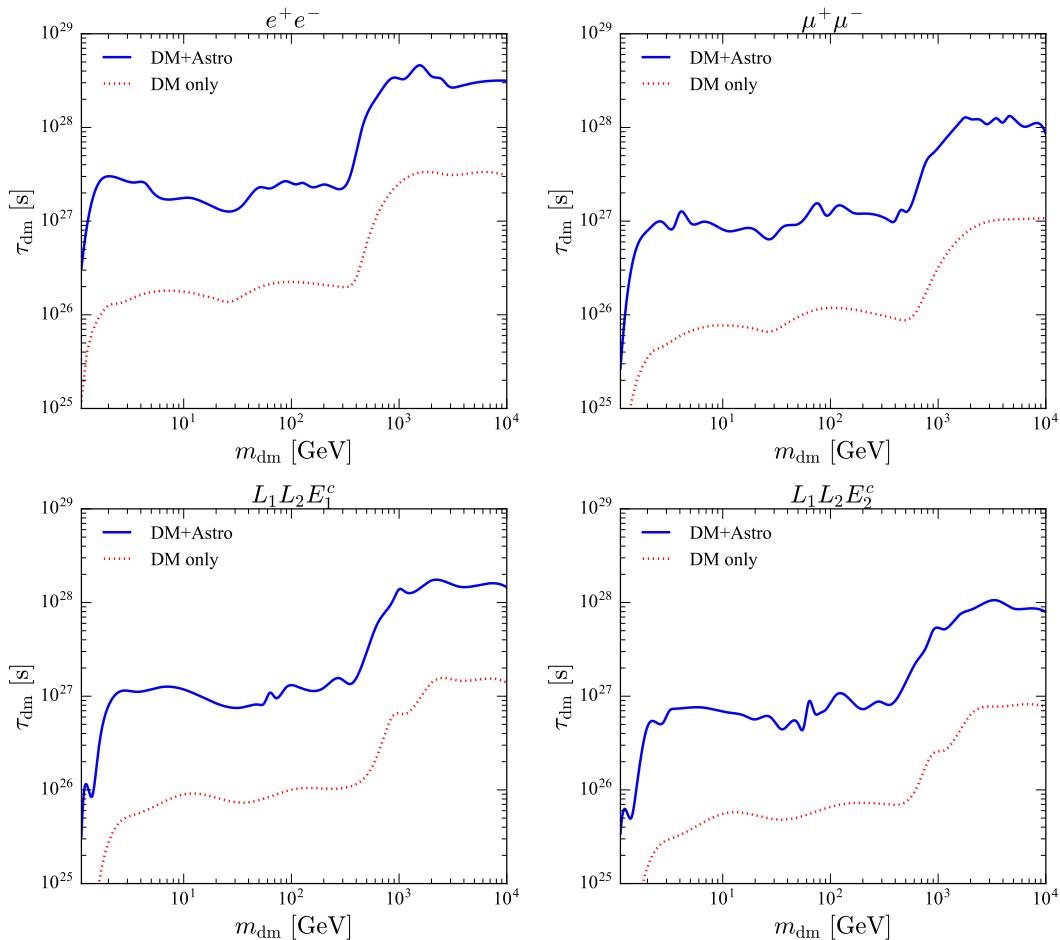


Figure 7. Lower limits on dark matter lifetime for leptonic channels due to cross correlation between the EGRB and five galaxy catalogs. The solid curves are the limits as the result of analysis that takes into account astrophysical contributions, while the dotted curves are the dark matter only analysis as shown in Figs. 3–5. For example, for $\mu^+\mu^-$ channel, the obtained results are better than the latest limit [42] given from dwarf galaxies by a few factors.

of the cosmic-ray anti-proton as mentioned in the previous subsection. Our present result for $W^\pm\mu^\mp$ final state excludes possibility to explain the anti-proton excess even in MAX or MED models.⁶ As stressed before, including the impact of the IC gamma rays is crucial to get this conclusion.

Finally we give results for annihilation cases. Figure 10 shows the same result as Fig. 6 but taking astrophysical components into account. Similar to decaying cases given in Figs. 7–9, the constraints become more stringent by an order of magnitude compared to those by taking only dark matter component. For a reference, a line $\langle\sigma v\rangle = 3 \times 10^{-26} \text{ cm}^3 \text{ s}^{-1}$, which is required value for the conventional thermal WIMP production scenario, is also shown in the plot. It is found that the mass region $m_{\text{dm}} \lesssim 100 \text{ GeV}$ is excluded for the thermal WIMP mainly annihilating to $b\bar{b}$ or $\tau^+\tau^-$. Namely the cross-correlating analysis is beginning to

⁶It might be possible to find loophole for the constraint, *e.g.*, considering unconventional propagation model or spectrum for astrophysical proton source. Our discussion is based on conventional cases.

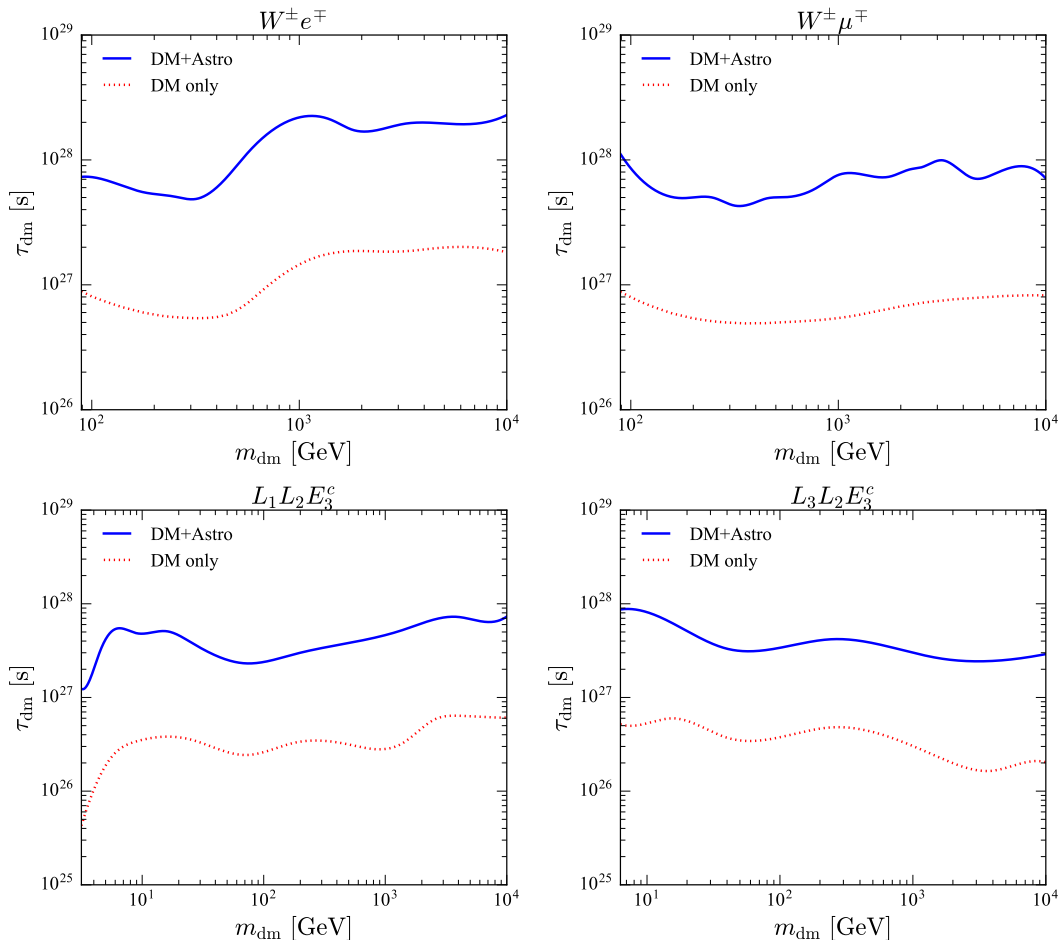


Figure 8. The same as Fig. 7 but for the hadroleptonic channels.

investigate the weak-scale mass region of the WIMP dark matter.

6 Conclusions

Indirect detection of dark matter via cosmic rays is a promising way for the probe of the nature of dark matter. Anomalous fluxes in cosmic-ray positron and anti-proton recently reported by AMS-02 collaboration indicate the signal of decaying or annihilating dark matter with a mass of 1–10 TeV. On the other hand, there is an alternative solution for the anomalies, such as nearby pulsars for the positron flux or known inner-galactic activities for anti-proton. Extragalactic gamma-ray background has a potential to clarify the situation. In the dark matter scenarios suggested to explain the anti-proton excess, lots of gamma rays are produced due to the cascade decay of the final state products. Even in the leptonic final states motivated by the positron excess, gamma rays are produced via final state radiation or inverse-Compton process. On observational side, gamma-ray data has been accumulated, which enables us to study their spatial distribution with better accuracy. In addition, the astrophysical sources for extragalactic gamma rays, such as blazars, star-forming galaxies, etc., have been identified due to the recent development of the observations.

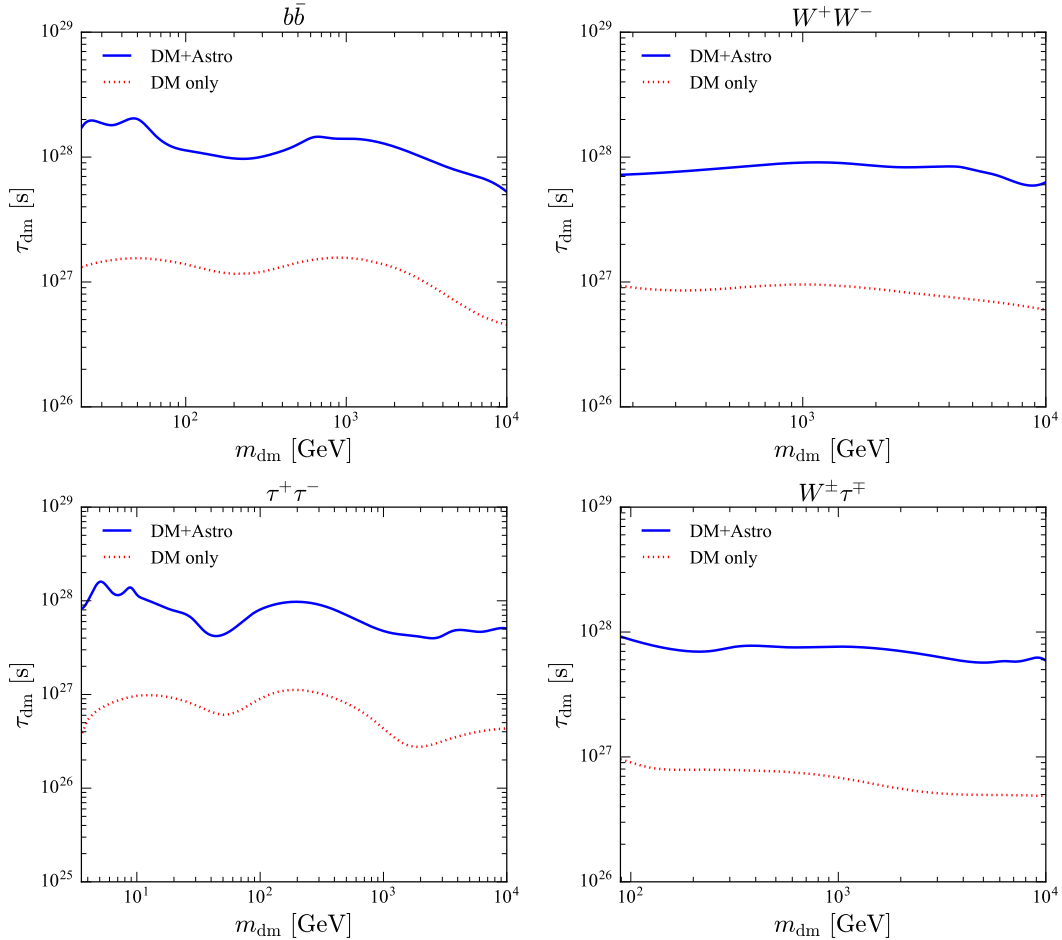


Figure 9. The same as Fig. 7 but for the hadronic channels.

In the article we compute the cross correlation of gamma rays from dark matter with local galaxy catalogs for the study of dark matter. In the previous studies which use the same technique, gamma rays from dark matter in inverse-Compton scattering were neglected, which we have included in the present work. We have found that the inverse-Compton scattering due to the CMB photon is crucial to constrain TeV scale dark matter, and consequently most stringent constrains has been obtained, especially on leptonic channels of the decay or annihilation of dark matter. We have done two types of analysis; computing the angular cross correlation of the gamma rays from i) only dark matter or from ii) both dark matter and astrophysical sources. To do comprehensive analysis, we have considered variety of final states, $l_i^+ l_i^-$, $\nu l_j^\pm l_k^\mp$, $W^\pm l_i^\mp$, $b\bar{b}$, $W^+ W^-$ for dark matter contribution. On the leptonic channels of decaying scenarios, lifetime of dark matter is constrained as $\tau_{\text{dm}} \gtrsim 10^{27}$ s and $\tau_{\text{dm}} \gtrsim 10^{28}$ s in analysis i) and ii), respectively, for $m_{\text{dm}} \gtrsim 1$ TeV. Thus, the decaying scenarios which are suggested to explain the positron or anti-proton excesses are excluded. This conclusion is robust since there is no uncertainty in the calculation of gamma rays from dark matter once decay channel is specified and that the we have based our discussion on the data of the observed astrophysical sources. We have checked consistency with the

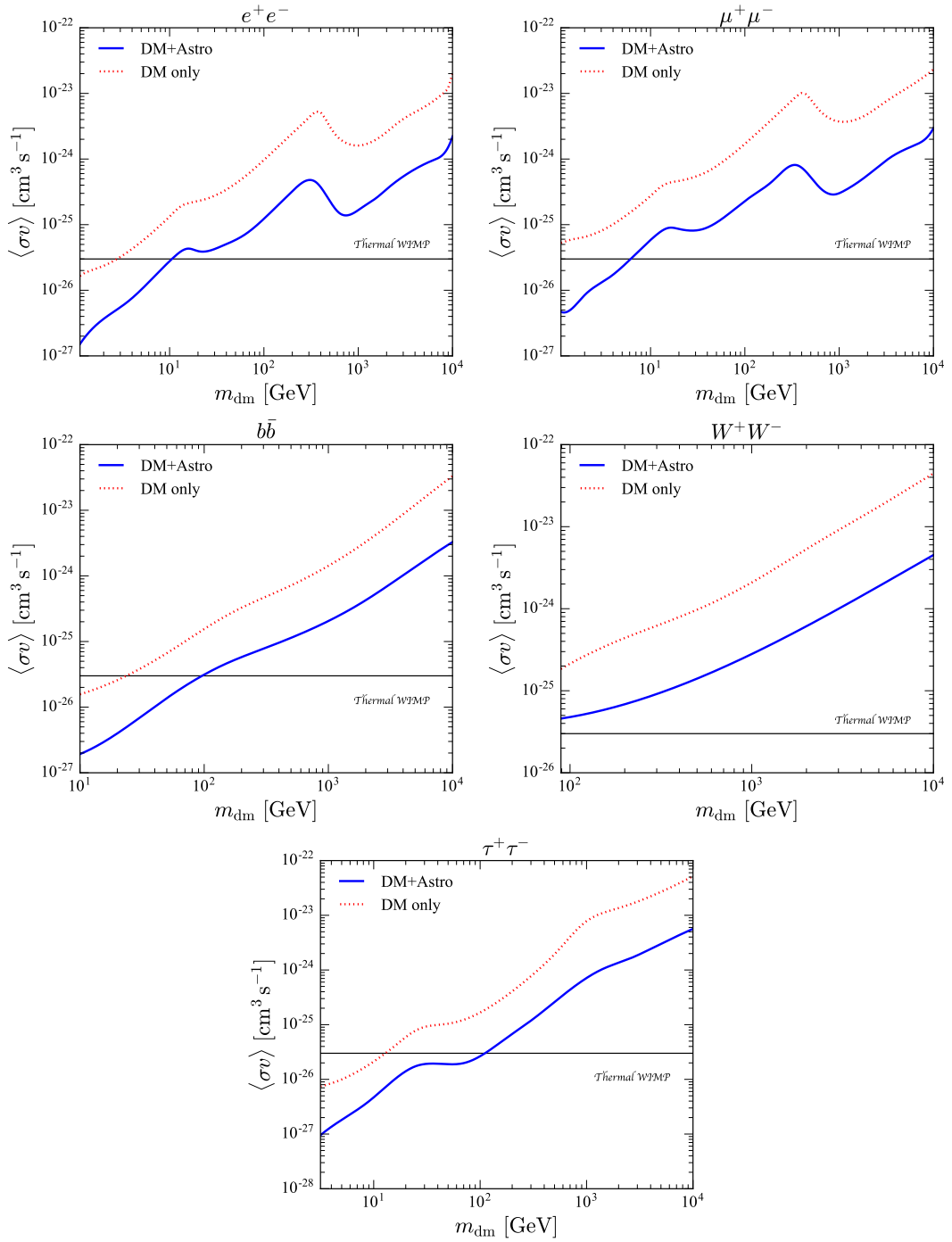


Figure 10. Upper limit on dark matter annihilation cross section due to cross correlation between the gamma-ray background and five galaxy catalogs. Line contents are the same as the decaying cases, *i.e.*, Figs. 7–9. Additionally, ‘Thermal WIMP’ line is included as in Fig. 6.

previous papers [16, 17], *i.e.*, the similar results are obtained for hadronic channels ($b\bar{b}$, W^+W^- , $\tau^+\tau^-$) and on leptonic channels ($\mu^+\mu^-$) in $m_{\text{dm}} \lesssim 1$ TeV region. For annihilating

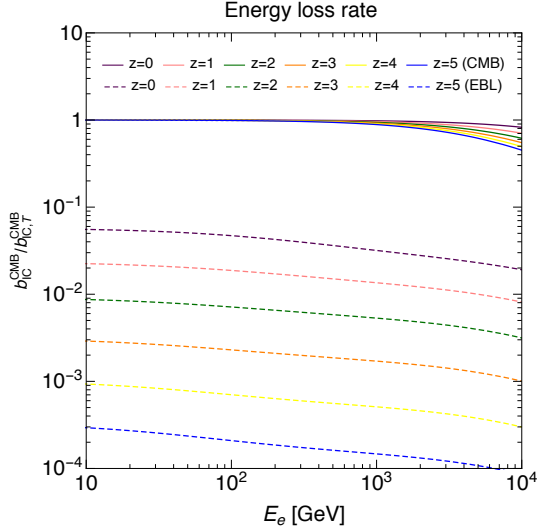


Figure 11. Energy loss rate of e^\pm as function of e^\pm energy, which is normalized by the analytic formula in Thomson limit. The energy loss rates due to the CMB (EBL) are given in solid (dotted) lines for $z = 0, 1, 2, 3, 4, 5$.

scenarios, similarly, the constraints get one to two orders of magnitude more stringent than the previous ones [16, 17] in TeV mass region. Besides, we have found that $m_{\text{dm}} \lesssim 100$ GeV is excluded for a WIMP dark matter which mainly annihilates into $b\bar{b}$ or $\tau^+\tau^-$, which is comparable constraint to that obtained by using dwarf spheroidal galaxies [19]. Those results are obtained by adopting the latest updates in the subhalo model [28], where the effects of tidal stripping are better treated compared to the past studies. Note, however, that the estimates are still subject to other uncertainties intrinsic to dark matter clustering down to extremely small scales (on the order of Earth mass), effects of baryons, etc., although future studies will address these issues. There is also a huge uncertainty in the computation of (anti-)proton flux in the galaxy. Thus, the constraint obtained here cannot exclude, for example, annihilating scenario to W^+W^- to explain the anti-proton excess. However, it is expected that more cosmic ray data by AMS-02 will reduce the uncertainty in the cosmic-ray propagation model, which will make it possible to test dark matter hypothesis for the origin of the anomalous anti-proton flux.

A Energy loss rate due to inverse-Compton scattering

In Fig. 11 we plot $b_{\text{IC}}^{\text{CMB}}(E_e, z)$ and $b_{\text{IC}}^{\text{EBL}}(E_e, z)$ as function of E_e normalized by the analytic expression in Thomson limit, $b_{\text{IC,T}}^{\text{CMB}}(E_e, z)$. For the energy loss under the CMB, it is seen that the analytic expression in the Thomson limit well agrees with the numerical result. However, in larger energy range $E_e \gtrsim 1$ TeV, which we are interested in the current study, the numerical result deviates from $b_{\text{IC,T}}^{\text{CMB}}(E_e, z)$ especially larger z . In the EBL, on the other hand, Thomson limit can not be applied. However, the energy loss due to the EBL is less than 5% compared to one due to the CMB. Thus the EBL itself merely affects our numerical study. The numerical results given in Figs. 3–6 (see “All” and “No EBL” in the figures) are consistent with this fact.

Acknowledgments

The authors thank M. Regis for useful discussions. This work was supported by the Netherlands Organization for Scientific Research (NWO) through Vidi grant (SA).

References

- [1] G. Aad *et al.* [ATLAS Collaboration], Phys. Lett. B **716**, 1 (2012) doi:10.1016/j.physletb.2012.08.020 [arXiv:1207.7214 [hep-ex]].
- [2] S. Chatrchyan *et al.* [CMS Collaboration], Phys. Lett. B **716**, 30 (2012) doi:10.1016/j.physletb.2012.08.021 [arXiv:1207.7235 [hep-ex]].
- [3] G. Hinshaw *et al.* [WMAP Collaboration], Astrophys. J. Suppl. **208**, 19 (2013) doi:10.1088/0067-0049/208/2/19 [arXiv:1212.5226 [astro-ph.CO]].
- [4] P. A. R. Ade *et al.* [Planck Collaboration], Astron. Astrophys. **571**, A16 (2014) doi:10.1051/0004-6361/201321591 [arXiv:1303.5076 [astro-ph.CO]].
- [5] P. A. R. Ade *et al.* [Planck Collaboration], arXiv:1502.01589 [astro-ph.CO].
- [6] F. Takayama and M. Yamaguchi, Phys. Lett. B **485**, 388 (2000) doi:10.1016/S0370-2693(00)00726-7 [hep-ph/0005214].
- [7] L. Accardo *et al.* [AMS Collaboration], Phys. Rev. Lett. **113** (2014) 121101. doi:10.1103/PhysRevLett.113.121101
- [8] AMS-02 collaboration, talks at the AMS DAYS AT CERN - The Future of Cosmic Ray Physics and Latest Results, April 15-17, 2015, CERN.
- [9] T. Linden and S. Profumo, Astrophys. J. **772**, 18 (2013) doi:10.1088/0004-637X/772/1/18 [arXiv:1304.1791 [astro-ph.HE]].
- [10] G. Giesen, M. Boudaud, Y. Gholini, V. Poulin, M. Cirelli, P. Salati and P. D. Serpico, JCAP **1509**, no. 09, 023 (2015) doi:10.1088/1475-7516/2015/09/023, 10.1088/1475-7516/2015/9/023 [arXiv:1504.04276 [astro-ph.HE]].
- [11] R. Kappl, A. Reinert and M. W. Winkler, JCAP **1510**, no. 10, 034 (2015) doi:10.1088/1475-7516/2015/10/034 [arXiv:1506.04145 [astro-ph.HE]].
- [12] K. Ishiwata, S. Matsumoto and T. Moroi, Phys. Lett. B **679**, 1 (2009) doi:10.1016/j.physletb.2009.07.004 [arXiv:0905.4593 [astro-ph.CO]].
- [13] S. Profumo and T. E. Jeltema, JCAP **0907**, 020 (2009) doi:10.1088/1475-7516/2009/07/020 [arXiv:0906.0001 [astro-ph.CO]].
- [14] S. Ando and K. Ishiwata, JCAP **1505**, no. 05, 024 (2015) doi:10.1088/1475-7516/2015/05/024 [arXiv:1502.02007 [astro-ph.CO]].
- [15] M. Ackermann *et al.* [Fermi-LAT Collaboration], Astrophys. J. **799**, 86 (2015) doi:10.1088/0004-637X/799/1/86 [arXiv:1410.3696 [astro-ph.HE]].
- [16] M. Regis, J. Q. Xia, A. Cuoco, E. Branchini, N. Fornengo and M. Viel, Phys. Rev. Lett. **114**, no. 24, 241301 (2015) doi:10.1103/PhysRevLett.114.241301 [arXiv:1503.05922 [astro-ph.CO]].
- [17] A. Cuoco, J. Q. Xia, M. Regis, E. Branchini, N. Fornengo and M. Viel, Astrophys. J. Suppl. **221**, no. 2, 29 (2015) doi:10.1088/0067-0049/221/2/29 [arXiv:1506.01030 [astro-ph.HE]].
- [18] M. Cirelli *et al.*, JCAP **1103**, 051 (2011) Erratum: [JCAP **1210**, E01 (2012)] doi:10.1088/1475-7516/2012/10/E01, 10.1088/1475-7516/2011/03/051 [arXiv:1012.4515 [hep-ph]].
- [19] M. Ackermann *et al.* [Fermi-LAT Collaboration], Phys. Rev. Lett. **115**, no. 23, 231301 (2015) doi:10.1103/PhysRevLett.115.231301 [arXiv:1503.02641 [astro-ph.HE]].

- [20] K. Hamaguchi, T. Moroi and K. Nakayama, Phys. Lett. B **747**, 523 (2015)
doi:10.1016/j.physletb.2015.06.041 [arXiv:1504.05937 [hep-ph]].
- [21] K. Ishiwata, S. Matsumoto and T. Moroi, Phys. Rev. D **78**, 063505 (2008)
doi:10.1103/PhysRevD.78.063505 [arXiv:0805.1133 [hep-ph]].
- [22] M. Ibe, S. Matsumoto, S. Shirai and T. T. Yanagida, Phys. Lett. B **741**, 134 (2015)
doi:10.1016/j.physletb.2014.12.016 [arXiv:1409.6920 [hep-ph]].
- [23] M. Cirelli, E. Moulin, P. Panci, P. D. Serpico and A. Viana, Phys. Rev. D **86**, 083506 (2012)
doi:10.1103/PhysRevD.86.083506, 10.1103/PhysRevD.86.109901 [arXiv:1205.5283
[astro-ph.CO]].
- [24] J. Q. Xia, A. Cuoco, E. Branchini and M. Viel, Astrophys. J. Suppl. **217**, no. 1, 15 (2015)
doi:10.1088/0067-0049/217/1/15 [arXiv:1503.05918 [astro-ph.CO]].
- [25] A. A. Abdo *et al.* [Fermi-LAT Collaboration], Phys. Rev. Lett. **104**, 101101 (2010)
doi:10.1103/PhysRevLett.104.101101 [arXiv:1002.3603 [astro-ph.HE]].
- [26] R. C. Gilmore, R. S. Somerville, J. R. Primack and A. Dominguez, Mon. Not. Roy. Astron.
Soc. **422**, 3189 (2012) [arXiv:1104.0671 [astro-ph.CO]].
- [27] T. Sjostrand, S. Mrenna and P. Z. Skands, JHEP **0605**, 026 (2006)
doi:10.1088/1126-6708/2006/05/026 [hep-ph/0603175].
- [28] R. Bartels and S. Ando, Phys. Rev. D **92**, no. 12, 123508 (2015)
doi:10.1103/PhysRevD.92.123508 [arXiv:1507.08656 [astro-ph.CO]].
- [29] F. Acero *et al.* [Fermi-LAT Collaboration], arXiv:1501.02003 [astro-ph.HE].
- [30] M. Ajello *et al.*, Astrophys. J. **800**, no. 2, L27 (2015) doi:10.1088/2041-8205/800/2/L27
[arXiv:1501.05301 [astro-ph.HE]].
- [31] M. Ackermann *et al.* [Fermi-LAT Collaboration], Astrophys. J. **755**, 164 (2012)
doi:10.1088/0004-637X/755/2/164 [arXiv:1206.1346 [astro-ph.HE]].
- [32] C. Gruppioni *et al.*, Mon. Not. Roy. Astron. Soc. **432**, 23 (2013) doi:10.1093/mnras/stt308
[arXiv:1302.5209 [astro-ph.CO]].
- [33] I. Tamborra, S. Ando and K. Murase, JCAP **1409**, 043 (2014)
doi:10.1088/1475-7516/2014/09/043 [arXiv:1404.1189 [astro-ph.HE]].
- [34] Y. Inoue, Astrophys. J. **733**, 66 (2011) doi:10.1088/0004-637X/733/1/66 [arXiv:1103.3946
[astro-ph.HE]].
- [35] M. Di Mauro, F. Calore, F. Donato, M. Ajello and L. Latronico, Astrophys. J. **780**, 161 (2014)
doi:10.1088/0004-637X/780/2/161 [arXiv:1304.0908 [astro-ph.HE]].
- [36] M. Fornasa and M. A. Sanchez-Conde, Phys. Rept. **598**, 1 (2015)
doi:10.1016/j.physrep.2015.09.002 [arXiv:1502.02866 [astro-ph.CO]].
- [37] M. Di Mauro and F. Donato, Phys. Rev. D **91**, no. 12, 123001 (2015)
doi:10.1103/PhysRevD.91.123001 [arXiv:1501.05316 [astro-ph.HE]].
- [38] S. Ando, A. Benoit-Lvy and E. Komatsu, Phys. Rev. D **90**, no. 2, 023514 (2014)
doi:10.1103/PhysRevD.90.023514 [arXiv:1312.4403 [astro-ph.CO]].
- [39] S. Ando, JCAP **1410**, no. 10, 061 (2014) doi:10.1088/1475-7516/2014/10/061 [arXiv:1407.8502
[astro-ph.CO]].
- [40] N. Fornengo and M. Regis, Front. Physics **2**, 6 (2014) doi:10.3389/fphy.2014.00006
[arXiv:1312.4835 [astro-ph.CO]].
- [41] V. Allevato, A. Finoguenov and N. Cappelluti, Astrophys. J. **797**, no. 2, 96 (2014)
doi:10.1088/0004-637X/797/2/96 [arXiv:1410.0358 [astro-ph.GA]].

- [42] M. G. Baring, T. Ghosh, F. S. Queiroz and K. Sinha, *Phys. Rev. D* **93**, no. 10, 103009 (2016) doi:10.1103/PhysRevD.93.103009 [arXiv:1510.00389 [hep-ph]].
- [43] L. Dugger, T. E. Jeltema and S. Profumo, *JCAP* **1012**, 015 (2010) doi:10.1088/1475-7516/2010/12/015 [arXiv:1009.5988 [astro-ph.HE]].
- [44] X. Huang, G. Vertongen and C. Weniger, *JCAP* **1201**, 042 (2012) doi:10.1088/1475-7516/2012/01/042 [arXiv:1110.1529 [hep-ph]].
- [45] F. Donato, N. Fornengo, D. Maurin and P. Salati, *Phys. Rev. D* **69**, 063501 (2004) doi:10.1103/PhysRevD.69.063501 [astro-ph/0306207].
- [46] F. Feroz, M. P. Hobson and M. Bridges, *Mon. Not. Roy. Astron. Soc.* **398**, 1601 (2009) doi:10.1111/j.1365-2966.2009.14548.x [arXiv:0809.3437 [astro-ph]].
- [47] F. Feroz and M. P. Hobson, *Mon. Not. Roy. Astron. Soc.* **384**, 449 (2008) doi:10.1111/j.1365-2966.2007.12353.x [arXiv:0704.3704 [astro-ph]].
- [48] F. Feroz, M. P. Hobson, E. Cameron and A. N. Pettitt, arXiv:1306.2144 [astro-ph.IM].